

(p,α) reactions on 1p, 2s-1d shell nuclei

F. Pellegrini, D. Trivisonno, S. Avon, R. Bianchin, and R. Rui  
 Istituto di Fisica dell' Università, Padova, Italy  
 and Istituto Nazionale di Fisica Nucleare, Sezione di Padova, Italy  
 (Received 1 March 1983)

The  $^{12}\text{C}(p,\alpha)^9\text{B}$  and  $^{32}\text{S}(p,\alpha)^{29}\text{P}$  reactions have been studied at incident energies of 42.77 and 41.9 MeV, respectively. The experimental (p,α) relative cross sections are well reproduced by distorted wave direct pickup calculations with a semimicroscopic form factor and current shell model wave functions. A comparison between (p,α) and ( $^3\text{He},d$ ) spectra on 1p and 2s-1d shell nuclei, leading to the same final nucleus, shows a clear evidence of a dominant pickup process over the knockout mechanism in the dynamics of the (p,α) reaction.

NUCLEAR REACTIONS, NUCLEAR STRUCTURE  $^{12}\text{C}(p,\alpha)^9\text{B}$ ,  $E = 42.77$  MeV,  $^{32}\text{S}(p,\alpha)^{29}\text{P}$ ,  $E = 41.9$  MeV, measured  $\sigma(E_x, \theta)$ ; natural targets. DWBA analysis. Calculated  $^9\text{B}$  energy levels,  $^{12}\text{C}(p,\alpha)^9\text{B}$  and  $^{32}\text{S}(p,\alpha)^{29}\text{P}$  spectroscopic strengths.

I. INTRODUCTION

In our previous investigations<sup>1-3</sup> we have emphasized the coherence property of the (p,α) reaction and its comparison with the single proton transfer (d,  $^3\text{He}$ ) reaction. The coherence property of the direct one step three-nucleon transfer (p,α) reaction is better understood by showing graphically, as in Fig. 1, the corresponding transition matrix element.

With a zero spin target nucleus  $A$ , only one total angular momentum transfer ( $J$ ) is allowed and the resulting matrix element is given by a coherent sum

$$\sum_{n'} \beta_n \langle f | V | i \rangle_n$$

over several transfers

$$[j_1 j_2 j_3]_J, [j_1^2 j_2]_J, \dots$$

corresponding to different internal states of the transferred nucleons. The  $\beta_n$  coefficients depend on these transfers and on the spectroscopic amplitudes. The interaction  $V$  between the incoming proton and the three nucleons at the nuclear surface causes the transition from the initial ( $i$ ) to the final ( $f$ ) state and the cross section  $\sigma$  is proportional to the square of the coherent sum, that is,

$$\sigma \propto \left| \sum_n \beta_n \langle f | V | i \rangle_n \right|^2.$$

The direct comparison between the (p,α) and (d,  $^3\text{He}$ ) reactions has led to another interesting feature for the three nucleon transfer reaction. Let us consider the  $(A+2)(p,\alpha)B$  reaction and the corresponding  $A(d, ^3\text{He})B$  reaction leading to the same final state of the residual nucleus  $B$ . In a simple picture, in which the  $(A+2)$  target nucleus is described as two neutrons outside the  $A$  core, the incoming proton can remove these two neutrons and a proton from the core, or only one external neutron and

two core nucleons, or three core nucleons. In the first case one hole states (1h), which are also excited in the ( $d, ^3\text{He}$ ) reaction, are formed, and in the other two cases one particle, two hole (1p-2h) or 2p-3h states, which have no counterpart in the ( $d, ^3\text{He}$ ) reaction, are obtained. If the wave function of the  $J$  state under study of the residual nucleus  $B$  is given by

$$\Psi(B) = \gamma_1 |1h\rangle + \gamma_2 |1p-2h\rangle + \gamma_3 |2p-3h\rangle + \dots,$$

with  $\gamma_2$  and  $\gamma_3 \ll \gamma_1$  we should expect a similar behavior between (p,α) and (d,  $^3\text{He}$ ) reactions. On the other hand if  $\gamma_2$  or  $\gamma_3$  is comparable with  $\gamma_1$ , due to the coherence property of the (p,α) reaction, we should expect substantial differences between (p,α) and (d,  $^3\text{He}$ ) reactions. This large difference has been obtained experimentally in the case of  $^{34}\text{S}(p,\alpha)^{31}\text{P}$  and  $^{32}\text{S}(d, ^3\text{He})^{31}\text{P}$  reactions.<sup>1</sup>

In order to investigate further the (p,α) mechanism we have performed the present experiment on other nuclei in the 1p and 2s-1d region at incident energies of 42.77 and 41.9 MeV, respectively. The choice of  $^{12}\text{C}(p,\alpha)^9\text{B}$  and  $^{32}\text{S}(p,\alpha)^{29}\text{P}$  reactions was motivated by the availability of current shell model wave functions for target and residual nuclei which allow a quantitative analysis necessary for the understanding of the reaction mechanism. Furthermore, we would like in the present paper to investigate the importance of a knockout process for the dynamics of the

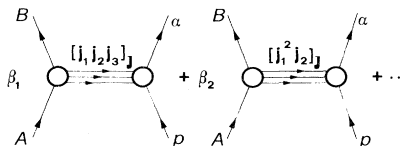


FIG. 1. Diagram illustrating the (p,α) pickup process.

(p, $\alpha$ ) reaction mechanism in the  $1p$  and  $2s-1d$  nuclear region.

## II. EXPERIMENTAL PROCEDURE

The momentum analyzed beam from the Milano azimuthally varying field cyclotron provided the source of the proton beam. The scattered particles were detected by silicon surface barrier detectors as in Ref. 3. In the case of  $^{32}\text{S}(p,\alpha)^{29}\text{P}$  we used counter telescopes which consisted of two silicon surface barrier detectors with the last one employed as a rejector of the scattered protons. The target for the  $^{12}\text{C}(p,\alpha)^9\text{B}$  experiment was a carbon foil of nominal thickness of  $200 \mu\text{g}/\text{cm}^2$ . This thickness was checked by a transmission experiment using an  $\alpha$  source of  $^{241}\text{Am}$ . By measuring the loss of energy of the most intense 5.486 MeV  $\alpha$  particles peak through the carbon foil, the real thickness was determined to be  $185 \pm 16 \mu\text{g}/\text{cm}^2$ . For the  $^{32}\text{S}(p,\alpha)^{29}\text{P}$  experiment we used a solid CdS target evaporated onto a  $100 \mu\text{g}/\text{cm}^2$  carbon backing and a gas target cell containing chemically pure (99.98%)  $\text{SO}_2$ . The gas pressure was 114 Torr corresponding to thicknesses of  $180 \mu\text{g}/\text{cm}^2$  and  $60 \mu\text{g}/\text{cm}^2$ , for the smallest and the largest angle of scattering observed in the experiment. The windows of the gas cell were of Kapton 50 (DuPont registered trademark)  $12.5 \mu\text{m}$  thick foils. The pressure and temperature of the gas were continuously checked during the experiment. Measurements were taken in the angular interval  $10-60$  degrees in the laboratory system in steps of 2.5 and 5 degrees for the  $^{12}\text{C}(p,\alpha)^9\text{B}$  reaction and in the angular interval  $10-68$  degrees for the  $^{32}\text{S}(p,\alpha)^{29}\text{P}$  reaction in 4 degree steps.

## III. EXPERIMENTAL RESULTS AND DISCUSSION

### A. $^{12}\text{C}(p,\alpha)^9\text{B}$ reaction at 42.77 MeV

A typical pulse height spectrum is shown in Fig. 2. The energy resolution of the ground state peak is of the order of 100 keV. The peaks are labeled by their excitation energies, widths, spins, and parities. We observe that the strongest transitions populate only negative parity states; the 2.79 MeV  $J^\pi = (\frac{3}{2}^+, \frac{5}{2}^+)$  state is very weakly excited. This property has been observed in other (p, $\alpha$ ) reactions on  $1p$  shell nuclei, as in the  $^{16}\text{O}(p,\alpha)^{13}\text{N}$  reaction studied at 54.1 MeV bombarding energy.<sup>4</sup> In this reaction the strongest transitions populate only negative parity states in the final  $^{13}\text{N}$  nucleus with cross sections which are one or two orders of magnitude larger than those of positive parity states. Such an effect suggests a dominant pickup over knockout mechanism with excitation of pure  $p$  state levels.

In a knockout mechanism we should observe transitions to both types of levels, in which the transferred proton can be captured into  $1p$  or  $2s-1d$  orbits. However other properties of the (p, $\alpha$ ) reactions on  $1p$  and  $2s-1d$  target nuclei, which suggest a strong indication of a dominant pickup over the knockout process, will be discussed later. Figure 3 shows the angular distributions with the DWBA curves of  $\alpha$  particles leading to the ground and excited states of  $^9\text{B}$ . The DWBA calculations were carried out with the code DWUCK4 written by Kunz, using semimicroscopic zero range form factors as in our previous works.<sup>1,2</sup> The optical model parameters for the  $^{12}\text{C} + p$  and  $^9\text{B} + \alpha$  channels were taken from Li and Hird in the analysis of the  $^{12}\text{C}(p,\alpha)^9\text{B}$  ground state transition at 44.5 MeV.<sup>5</sup> These parameters are shown in Table I. In a semimicroscopic description of the (p, $\alpha$ ) reaction we can express the differential cross section as

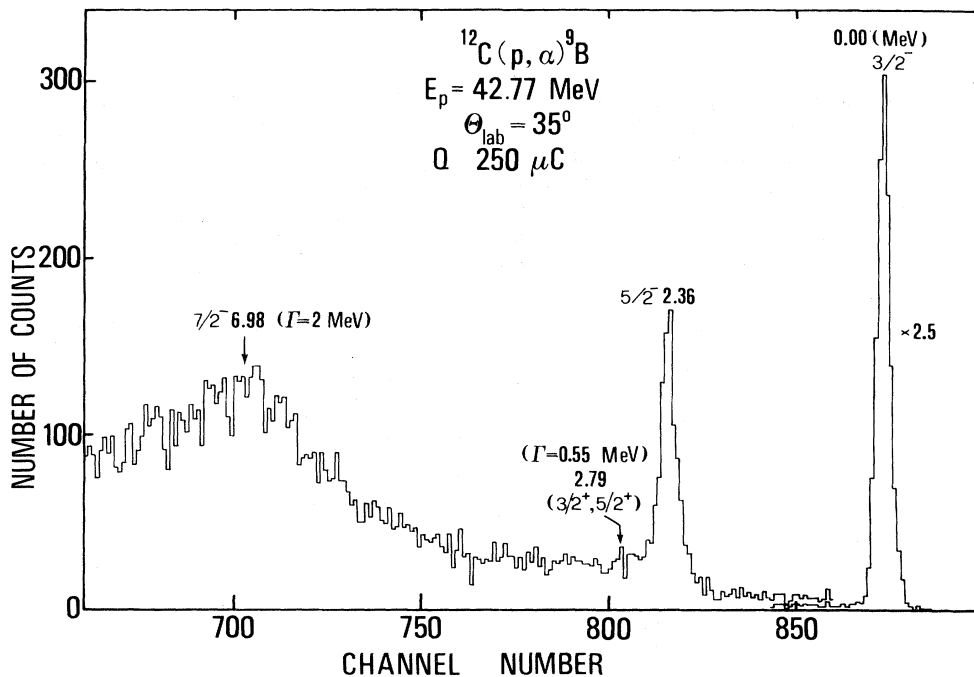


FIG. 2. Alpha spectrum from the  $^{12}\text{C}(p,\alpha)^9\text{B}$  reaction at  $E=42.77 \text{ MeV}$  and  $\theta_{\text{lab}}=35^\circ$ .

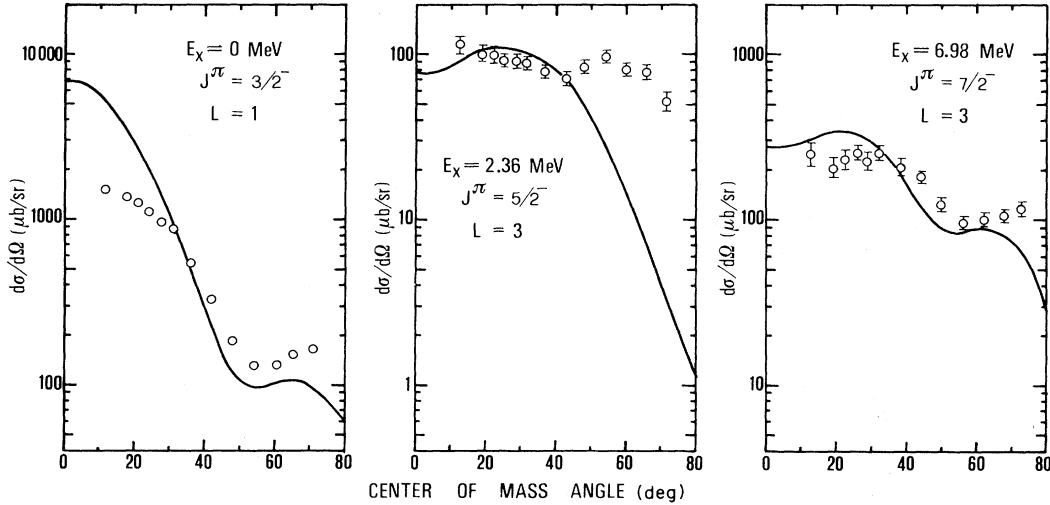


FIG. 3. Experimental  $^{12}\text{C}(p,\alpha)^9\text{B}$  differential cross sections and DWBA calculations for the ground ( $L=1$ ) state, and for the 2.36 MeV ( $L=3$ ) and 6.98 MeV ( $L=3$ ) states of  $^9\text{B}$ .

$$\left(\frac{d\sigma}{d\Omega}\right)^{NLJ} = D \left[ \sum_{\substack{\bar{N}, \bar{L}, \bar{S}, \bar{J} \\ \bar{T}, \bar{T}_3}} \left(\frac{A}{A-3}\right)^{N+L/2} \begin{Bmatrix} l_1 & s_1 & j_1 \\ l_2 & s_2 & j_2 \\ \bar{L} & \bar{S} & \bar{J} \end{Bmatrix} \begin{Bmatrix} l_3 & s_3 & j_3 \\ \bar{L} & \bar{S} & \bar{J} \\ L & \frac{1}{2} & J \end{Bmatrix} \right. \\ \left. \times \left(\frac{1}{2}\frac{1}{2}t_1t_2 \mid \bar{T}\bar{T}_3\right) \left(\frac{1}{2}\bar{T}t_3\bar{T}_3 \mid \frac{1}{2}, +\frac{1}{2}\right) \langle \bar{N}\bar{L} \mid n_1l_1n_2l_2 \rangle \langle NL \mid n_3l_3\bar{N}\bar{L} \rangle \sqrt{S_{LJT}} \right]^2 \\ \times (2J+1)^{-1} \sigma_{\text{DWUCK}}^{NLJ}(\theta).$$

The factor  $D$  is a normalization constant, the first term is the center of mass correction, and the curly brackets are the normalized  $9j$  symbols which perform the transformation from  $jj$  to  $LS$  coupling, parentheses and angular brackets are the isospin Clebsch-Gordan and Moshinsky coefficients which transform the dinucleon  $n_1l_1(\frac{1}{2}t_1)$ ,  $n_2l_2(\frac{1}{2}t_2)$  with orbital angular momentum  $\bar{L}$ , radial quantum number  $\bar{N}$ , and isospin  $(\bar{T}, \bar{T}_3)$ , and the  $n_3l_3(\frac{1}{2}t_3)$  nucleon to a triton with quantum numbers  $NLJ(\frac{1}{2}, +\frac{1}{2})$ . Finally, the  $\sqrt{S}$  is the spectroscopic amplitude for three nucleon transfer and  $\sigma(\theta)$  is the differential cross section as given by the code DWUCK.

## B. Shell model calculations

In order to calculate spectroscopic amplitudes, we have reproduced the calculations of Cohen and Kurath<sup>6</sup> and Amit and Katz,<sup>7</sup> who used effective interactions for the  $1p$  shell nuclei by a fitting procedure. The  $1p$  configurations involved in describing the  $^{12}\text{C}$  and  $^9\text{B}$  levels are, respectively,  $(1p_{3/2})^{8-n}(1p_{1/2})^n$  for  $^{12}\text{C}$  and  $(1p_{3/2})^{5-n}(1p_{1/2})^n$  for  $^9\text{B}$ , with  $0 \leq n \leq 4$ . The fifteen parameters for the two body interaction and the two single particle energies, which have been used in the calculations, are shown in Table II.

TABLE I. Optical model parameters used with the code DWUCK in the  $^{12}\text{C}(p,\alpha)^9\text{B}$  reaction.

| Channel               | $V$<br>(MeV) | $W$<br>(MeV) | $V_{\text{s.o.}}$<br>(MeV) | $r$<br>(fm) | $a$<br>(fm) | $r'$<br>(fm) | $a'$<br>(fm) | $r_c$<br>(fm) |
|-----------------------|--------------|--------------|----------------------------|-------------|-------------|--------------|--------------|---------------|
| $^{12}\text{C} + p$   | 37.6         | 5.2          |                            | 1.18        | 0.7         | 1.4          | 0.7          | 1.25          |
| $^9\text{B} + \alpha$ | 207.1        | 26           |                            | 1.54        | 0.475       | 1.54         | 0.475        | 1.4           |
| $^9\text{B} + t$      | a            | 0            | $\lambda=25$               | 1.3         | 0.25        |              |              | 1.4           |

<sup>a</sup>Adjusted to give the transferred triton a binding energy of  $-Q(p,\alpha) + 19.814$  MeV.

TABLE II.  $1p$  effective parameters used in the calculations of  $^{12}\text{C}$  and  $^9\text{B}$  energy levels.

| $2j_1$ | $2j_2$ | $2j_3$ | $2j_4$ | $JT$ | $\langle j_1 j_2   V   j_3 j_4 \rangle$<br>(MeV) |
|--------|--------|--------|--------|------|--|
| 3      | 3      | 3      | 3      | 01   | -4.12  |
| 3      | 3      | 3      | 3      | 21   | -1.28  |
| 3      | 3      | 3      | 3      | 10   | -5.50  |
| 3      | 3      | 3      | 3      | 30   | -5.64  |
| 1      | 1      | 1      | 1      | 01   | -2.27  |
| 1      | 1      | 1      | 1      | 10   | -3.79  |
| 3      | 3      | 3      | 1      | 21   | -1.71  |
| 3      | 3      | 3      | 1      | 10   | 0  |
| 3      | 3      | 1      | 1      | 01   | 2.01   |
| 3      | 3      | 1      | 1      | 10   | 0  |
| 3      | 1      | 3      | 1      | 11   | 2.68   |
| 3      | 1      | 3      | 1      | 21   | 0.38   |
| 3      | 1      | 3      | 1      | 10   | -8.82  |
| 3      | 1      | 3      | 1      | 20   | -3.67  |
| 3      | 1      | 1      | 1      | 10   | 1.89   |

$\epsilon_{1/2} = -2.49$  MeV     $\epsilon_{3/2} = 2.25$  MeV

The numerical evaluation of the matrix elements and the subsequent diagonalization of the matrices were performed using a VAX 11/780 computer. The calculated  $^9\text{B}$  energy level spectrum up to an excitation energy of 16 MeV is compared with the experimental one in Fig. 4. All levels reported in Ref. 7 are well reproduced as well as the contributions of the various  $jj$  configuration to the final states.

The shell model wave functions thus obtained were used for the calculation of the (p, $\alpha$ ) spectroscopic amplitudes and are shown in Table III. For these calculations we have taken the major components of the wave functions involved, which account for 98–99% of the  $^{12}\text{C}$  and  $^9\text{B}$  wave functions. The results are shown in Fig. 5 and compared with the experimental integrated cross sections. In addition, Table IV reports the summary of results from this  $^{12}\text{C}(p,\alpha)^9\text{B}$  reaction. The calculations reproduce fairly well the experimental spectrum proving the dominant character of the pickup mechanism for the dynamics of the (p, $\alpha$ ) reaction.

TABLE III. Spectroscopic amplitudes of the  $^{12}\text{C}(p,\alpha)^9\text{B}$  reaction. Configurations are assigned as  $[(j_1 j_2)_{J_1 T_1} (j_3 j_4)_{J_2 T_2}]_{J T}$ .

| $J^\pi, T$                   | $E_x$ (MeV) | Configuration                              | Spectroscopic amplitude |
|------------------------------|-------------|--|-------------------------|
| $\frac{3}{2}^-, \frac{1}{2}$ | 0           | $(1p_{3/2})_{3/2, 1/2}^3$                  | 1.320                   |
|                              |             | $[(1p_{3/2})(1p_{1/2})_{01}^2]_{3/2, 1/2}$ | 0.223                   |
|                              |             | $[(1p_{3/2})(1p_{1/2})_{10}^2]_{3/2, 1/2}$ | 0.039                   |
|                              |             | $[(1p_{3/2})_{10}^2(1p_{1/2})]_{3/2, 1/2}$ | -0.018                  |
|                              |             | $[(1p_{3/2})_{21}^2(1p_{1/2})]_{3/2, 1/2}$ | -0.070                  |
| $\frac{5}{2}^-, \frac{1}{2}$ | 2.36        | $(1p_{3/2})_{5/2, 1/2}^3$                  | 0.872                   |
|                              |             | $[(1p_{3/2})_{21}^2(1p_{1/2})]_{5/2, 1/2}$ | -0.198                  |
|                              |             | $[(1p_{3/2})_{30}^2(1p_{1/2})]_{5/2, 1/2}$ | -0.122                  |
|                              |             | $[(1p_{3/2})(1p_{1/2})_{10}^2]_{5/2, 1/2}$ | -0.046                  |
| $\frac{7}{2}^-, \frac{1}{2}$ | 6.98        | $(1p_{3/2})_{7/2, 1/2}^3$                  | -1.945                  |
|                              |             | $[(1p_{3/2})_{30}^2(1p_{1/2})]_{7/2, 1/2}$ | -0.365                  |

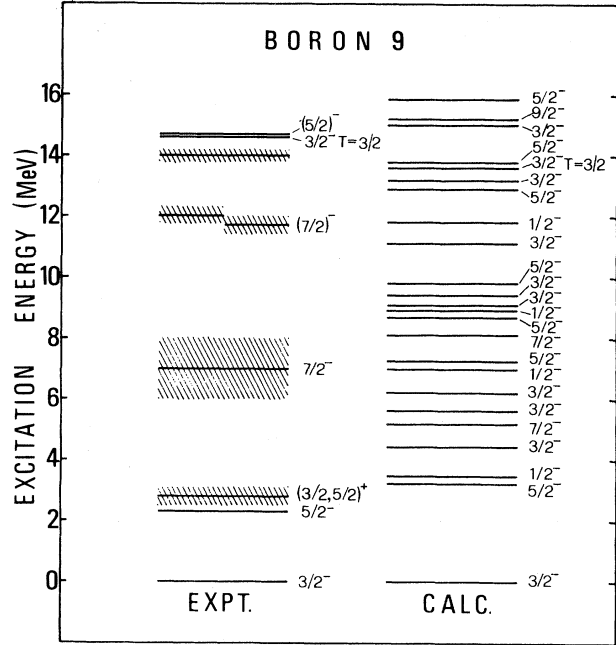


FIG. 4. A comparison between calculated and observed levels in  $^9\text{B}$  up to a 16 MeV excitation energy.

### C. The $^{32}\text{S}(p,\alpha)^{29}\text{P}$ reaction at 41.9 MeV

Spectra recorded at a laboratory angle of 20 degrees with the  $\text{SO}_2$  gas and  $\text{CdS}$  solid target are shown in Fig. 6. Up to a 3.5 MeV excitation energy, strong excitation is observed only for the  $J^\pi = 5/2^+$ , 1.95 MeV and  $J^\pi = \frac{1}{2}^+$  ground states. Figure 7 reports the experimental angular distributions with the DWBA curves. The optical model parameters used in the calculations are the same as those in the  $^{30}\text{Si}(p,\alpha)^{27}\text{Al}$  reaction at 40.75 MeV (Ref. 2) and are listed in Table V.

In order to calculate spectroscopic amplitudes we have

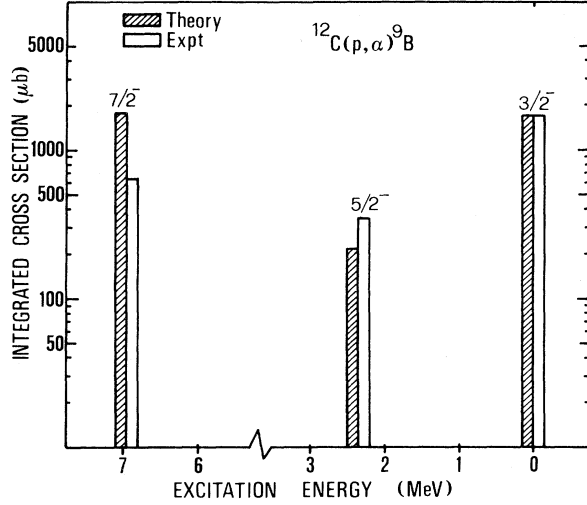


FIG. 5. Comparison of calculated and experimental integrated cross sections for the  $^{12}\text{C}(p,\alpha)^9\text{B}$  reaction.

taken the current shell model wave functions of  $2s-1d$  shell nuclei from the literature.<sup>8,9</sup> In particular for the  $^{32}\text{S}$  ground state we have taken the wave function reported in Ref. 8, with the major components, which account for 75% of the wave function, described by the following configurations:

$$0.623[(d_{5/2})_{00}^{12}(s_{1/2})_{00}^4] \\ -0.444\{[(d_{5/2})_{00}^{12}(s_{1/2})_{00}^2](d_{3/2})_{00}^2\} \\ -0.408\{[(d_{5/2})_{01}^{10}(s_{1/2})_{00}^4]_{01}(d_{3/2})_{01}^2\}_{00}.$$

For  $^{29}\text{P}$  we have taken the wave functions of Ref. 9.

The transfers involved in the present experiment with the corresponding amplitudes are shown in Table VI. The results are shown in Fig. 8 and compared with the experimental integrated cross sections. Finally, in Table VII is reported the summary of results from the  $^{32}\text{S}(p,\alpha)^{29}\text{P}$  reaction. The calculations reproduce well the experimental spectrum, demonstrating once more a dominant pickup reaction mechanism for the  $(p,\alpha)$  reaction at 40 MeV in the  $2s-1d$  nuclear region.

TABLE IV. Summary of results from the  $^{12}\text{C}(p,\alpha)^9\text{B}$  reaction.

| $E_x$ (MeV) | $J^\pi$         | $L$ | Integrated cross section |                                      | Angular interval of integration (lab) |
|-------------|-----------------|-----|--------------------------|--------------------------------------|---------------------------------------|
|             |                 |     | Expt. ( $\mu\text{b}$ )  | Calc. <sup>a</sup> ( $\mu\text{b}$ ) |                                       |
| 0           | $\frac{3}{2}^-$ | 1   | $1694 \pm 17$            | 1694                                 | 10–60                                 |
| 2.36        | $\frac{5}{2}^-$ | 3   | $344 \pm 69$             | 206                                  | 10–60                                 |
| 6.98        | $\frac{7}{2}^-$ | 3   | $644 \pm 200$            | 1778                                 | 10–60                                 |

<sup>a</sup>The calculated cross section has been integrated in the same angular interval as the experimental one using a normalized factor  $D=2343$ .

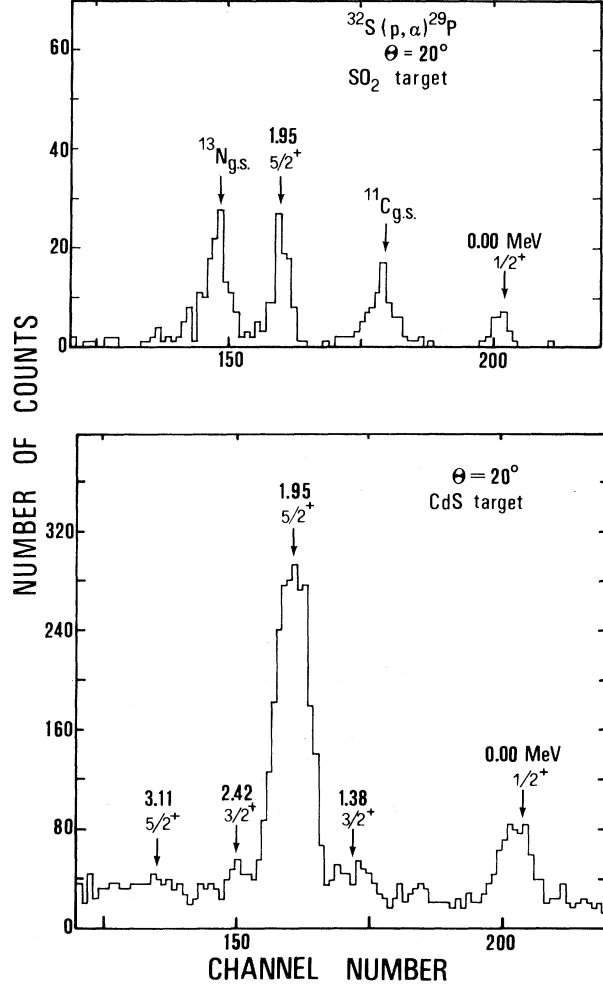


FIG. 6. Alpha spectra from the  $^{32}\text{S}(p,\alpha)^{29}\text{P}$  reaction at  $E=41.9$  MeV and  $\theta_{\text{lab}}=20^\circ$ , obtained with a  $\text{SO}_2$  gas and CdS target.

#### D. Knockout mechanism in the $(p,\alpha)$ reaction on $1p$ and $2s-1d$ shell nuclei

We remarked previously that the  $(p,\alpha)$  reactions on  $1p$  shell nuclei are characterized at low excitation energy by

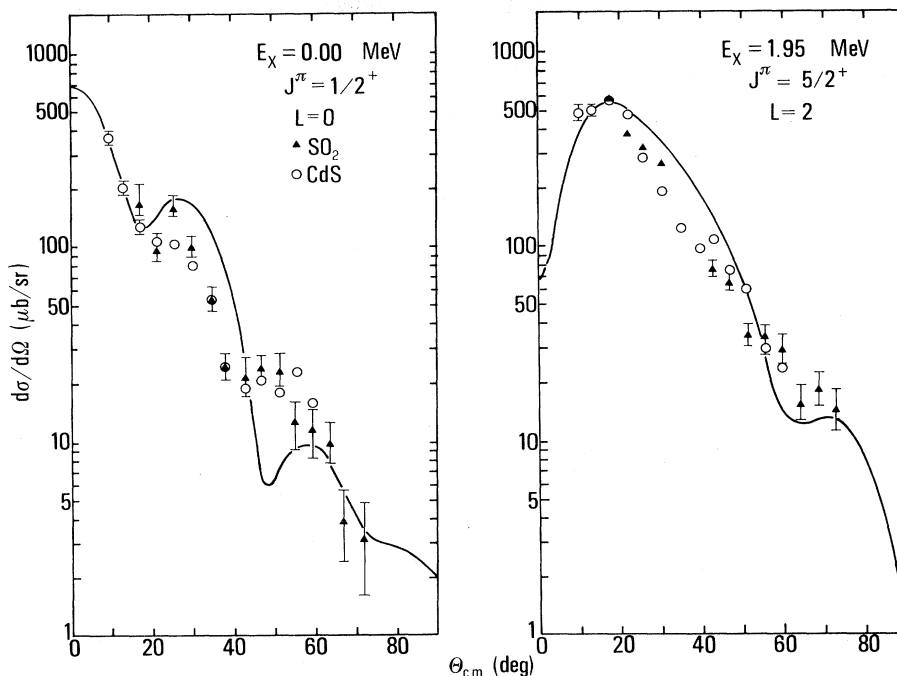


FIG. 7. Experimental  $^{32}\text{S}(p,\alpha)^{29}\text{P}$  cross sections and DWBA calculations with optical model parameters described in Table V.

spectra in which the positive parity states are less excited (one or two orders of magnitude) than the negative parity states. This property has been interpreted as a proof of a pickup mechanism dominant over the knockout process which would have allowed alpha transitions to both parity states. The diagram for alpha particle knockout in a (p, $\alpha$ ) reaction is shown in Fig. 9.

As we can see, the target, in the vicinity of the incoming proton, dissociates onto an alpha particle and a core C. Then the alpha particle interacts with the incident proton in the field of the core through an effective p- $\alpha$  interaction. The proton combines with the core to give the final nucleus B, while the alpha particle leaves the residual nucleus. In order to see the importance of such a diagram in describing the dynamics of a (p, $\alpha$ ) reaction, it is interesting to compare spectra obtained in  $A(p,\alpha)B$  and  $C(^3\text{He},d)B$  reactions. If the  $\alpha$  particle plays a spectator role in the diagram of Fig. 9 the comparison of these two spectra should give information about the reaction mechanism. In this hypothesis the (p, $\alpha$ ) and ( $^3\text{He},d$ ) spectra on the same final nuclei should be similar. On the other hand if the al-

pha particle is emitted from many different states of the target nucleus with different angular momenta, the comparison of the two (p, $\alpha$ ) and corresponding ( $^3\text{He},d$ ) spectra will be more complicated and difficult to be clearly interpreted.

With this aim we have considered the following (p, $\alpha$ ) reactions: the  $^{16}\text{O}(p,\alpha)^{13}\text{N}$  at 54.1 MeV,<sup>4</sup> the  $^{30}\text{Si}(p,\alpha)^{27}\text{Al}$  at 40.75 MeV,<sup>2</sup> the  $^{32}\text{S}(p,\alpha)^{29}\text{P}$  present experiment and the  $^{34}\text{S}(p,\alpha)^{31}\text{P}$  at 35.5 MeV.<sup>1</sup> For the corresponding ( $^3\text{He},d$ ) reactions to be compared we have taken, respectively,  $^{12}\text{C}(^3\text{He},d)^{13}\text{N}$  at 19.6 MeV,<sup>10</sup> the  $^{26}\text{Mg}(^3\text{He},d)^{27}\text{Al}$  at 17.85 MeV,<sup>11</sup> the  $^{28}\text{Si}(^3\text{He},d)^{29}\text{P}$  at 38.5 MeV,<sup>12</sup> and the  $^{30}\text{Si}(^3\text{He},d)^{31}\text{P}$  at 17.85 MeV.<sup>11</sup>

Figure 10 shows the first direct comparison between the  $^{16}\text{O}(p,\alpha)^{13}\text{N}$  and the  $^{12}\text{C}(^3\text{He},d)^{13}\text{N}$  reactions, where the maximum differential cross sections expressed in arbitrary units are compared. We observe peculiar differences. The largest discrepancy is in the excitation of negative parity states by the (p, $\alpha$ ) reaction and of positive parity states by the ( $^3\text{He},d$ ) reaction. In other words, if a state is excited in (p, $\alpha$ ), it is not in the corresponding ( $^3\text{He},d$ ) and vice versa.

TABLE V. Optical model parameters used with the code DWUCK in the  $^{32}\text{S}(p,\alpha)^{29}\text{P}$  reaction.

| Channel                  | $V$<br>(MeV) | $W$<br>(MeV) | $W_D$<br>(MeV) | $W_{s.o.}$<br>(MeV) | $r$<br>(fm) | $a$<br>(fm) | $r'$<br>(fm) | $a'$<br>(fm) | $r_{s.o.}$<br>(fm) | $a_{s.o.}$<br>(fm) | $r_c$<br>(fm) |
|--------------------------|--------------|--------------|----------------|---------------------|-------------|-------------|--------------|--------------|--------------------|--------------------|---------------|
| $^{32}\text{S} + p$      | 43           | 4.89         | 2.17           | 4.88                | 1.17        | 0.673       | 1.33         | 0.575        | 1.07               | 0.78               | 1.25          |
| $^{29}\text{P} + \alpha$ | 145          | 16           |                |                     | 1.22        | 0.7         | 1.76         | 0.42         |                    |                    | 1.4           |
| $^{29}\text{P} + t$      | a            | 0            |                | $\lambda=25$        | 1.25        | 0.65        |              |              |                    |                    | 1.4           |

<sup>a</sup>Adjusted to give the transferred triton a binding energy of  $-Q(p,\alpha) + 19.814$  MeV.

TABLE VI. Spectroscopic amplitudes of the  $^{32}\text{S}(p,\alpha)^{29}\text{P}$  reaction. Configurations are assigned as  $[(j_1 j_2)_{J_1 T_1} j_3]_{J, T}$ .

| $J^\pi, T$                   | $E_x$ (MeV) | Configuration                                    | Spectroscopic amplitude |  |  |
|------------------------------|-------------|--|-------------------------|--|--|
| $\frac{1}{2}^+, \frac{1}{2}$ | 0           | $(2s_{1/2})_{1/2, 1/2}^3$                        | -1.013                  |  |  |
|                              |             | $[(1d_{5/2})_{01}^2(2s_{1/2})]_{1/2, 1/2}$       | -0.646                  |  |  |
|                              |             | $[(1d_{5/2})_{10}^2(2s_{1/2})]_{1/2, 1/2}$       | -0.259                  |  |  |
|                              |             | $[(2s_{1/2})(1d_{3/2})_{01}^2]_{1/2, 1/2}$       | -0.609                  |  |  |
|                              |             | $[(1d_{5/2}2s_{1/2})_{21}(1d_{3/2})]_{1/2, 1/2}$ | -0.120                  |  |  |
|                              |             | $[(1d_{5/2})_{21}^2(1d_{3/2})]_{1/2, 1/2}$       | -0.039                  |  |  |
| $\frac{3}{2}^+, \frac{1}{2}$ | 1.38        | $[(1d_{5/2})(2s_{1/2})_{10}^2]_{3/2, 1/2}$       | -0.629                  |  |  |
|                              |             | $[(2s_{1/2})_{01}^2(1d_{3/2})]_{3/2, 1/2}$       | -0.182                  |  |  |
|                              |             | $[(1d_{3/2})_{01}^2(1d_{3/2})]_{3/2, 1/2}$       | 0.074                   |  |  |
|                              |             | $[(1d_{5/2}2s_{1/2})_{21}(1d_{3/2})]_{3/2, 1/2}$ | -0.063                  |  |  |
|                              |             | $[(1d_{5/2})(2s_{1/2})_{01}^2]_{5/2, 1/2}$       | -1.360                  |  |  |
|                              |             | $(1d_{5/2})_{5/2, 1/2}^3$                        | -0.949                  |  |  |
| $\frac{5}{2}^+, \frac{1}{2}$ | 1.95        | $[(1d_{5/2})(2s_{1/2})_{10}^2]_{5/2, 1/2}$       | 0.662                   |  |  |
|                              |             | $[(1d_{5/2})_{30}^2(2s_{1/2})]_{5/2, 1/2}$       | 0.455                   |  |  |
|                              |             | $[(1d_{5/2})_{21}^2(2s_{1/2})]_{5/2, 1/2}$       | 0.380                   |  |  |
|                              |             | $[(1d_{5/2})(1d_{3/2})_{01}^2]_{5/2, 1/2}$       | -0.266                  |  |  |
|                              |             | $[(1d_{5/2}2s_{1/2})_{21}(1d_{3/2})]_{5/2, 1/2}$ | 0.084                   |  |  |
|                              |             | $[(1d_{5/2})(2s_{1/2})_{10}^2]_{3/2, 1/2}$       | -0.937                  |  |  |
|                              |             | $[(1d_{5/2})_{21}^2(2s_{1/2})]_{3/2, 1/2}$       | -0.373                  |  |  |
|                              |             | $(1d_{5/2})_{3/2, 1/2}^3$                        | -0.240                  |  |  |
|                              |             | $[(1d_{5/2}2s_{1/2})_{21}(1d_{3/2})]_{3/2, 1/2}$ | 0.319                   |  |  |
|                              |             | $[(1d_{5/2})_{21}^2(1d_{3/2})]_{3/2, 1/2}$       | 0.058                   |  |  |
|                              |             | $[(1d_{5/2})_{01}^2(1d_{3/2})]_{3/2, 1/2}$       | -0.048                  |  |  |
|                              |             | $[(2s_{1/2})_{01}^2(1d_{3/2})]_{3/2, 1/2}$       | -0.044                  |  |  |
| $\frac{3}{2}^+, \frac{1}{2}$ | 2.42        | $[(1d_{5/2})(2s_{1/2})_{10}^2]_{5/2, 1/2}$       | 0.658                   |  |  |
|                              |             | $[(1d_{5/2}2s_{1/2})_{21}(1d_{3/2})]_{5/2, 1/2}$ | -0.482                  |  |  |
|                              |             | $[(1d_{5/2})_{21}^2(1d_{3/2})]_{5/2, 1/2}$       | -0.181                  |  |  |
|                              |             | $[(1d_{5/2})_{41}^2(1d_{3/2})]_{5/2, 1/2}$       | 0.057                   |  |  |
|                              |             | $\frac{5}{2}^+, \frac{1}{2}$                     | 3.11                    |  |  |

This is a clear evidence that the dynamics of  $(p,\alpha)$  reaction is based on a pickup mechanism and it is in contrast with the prediction of a knockout process in which the transferred proton can go mostly in empty orbits, as it

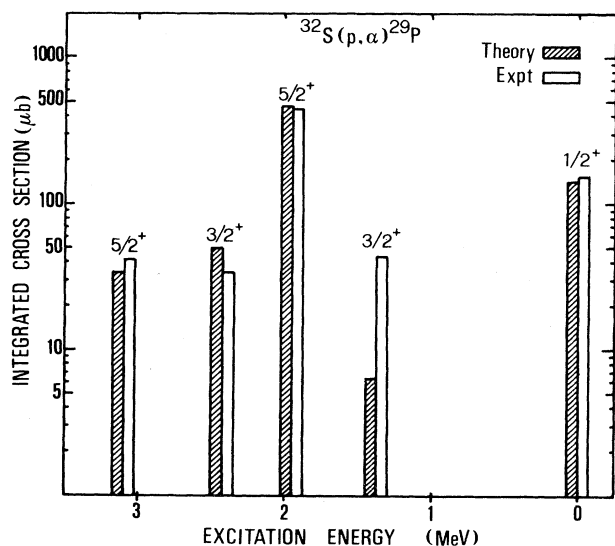


FIG. 8. Comparison of calculated and experimental integrated cross sections for the  $^{32}\text{S}(p,\alpha)^{29}\text{P}$  reaction.

does in the  $(^3\text{He},d)$  reaction. Figures 11–13 show the comparison of  $(p,\alpha)$  and the corresponding  $(^3\text{He},d)$  reactions on  $2s$ - $1d$  nuclei. We again observe the same peculiar differences noted previously. For instance, in Fig. 11 these features are observed for the  $J^\pi = \frac{1}{2}^+$  0.843 MeV,  $J^\pi = \frac{3}{2}^+$  2.98 MeV, and  $J^\pi = \frac{5}{2}^+$  3.00 MeV states of the residual nucleus  $^{27}\text{Al}$ .

In Fig. 12 the difference in the  $(p,\alpha)$  and  $(^3\text{He},d)$  spectra is limited for the  $J^\pi = \frac{3}{2}^+$  and  $J^\pi = \frac{5}{2}^+$  at 1.38 and 1.95 MeV excitation energies, respectively. Finally, Fig. 13 is rich with differences between the two spectra. In fact we observe a large excitation in one reaction and a low excitation for the same state in the other reaction. This hap-

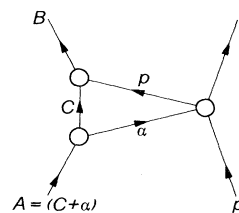


FIG. 9. Diagram illustrating the  $(p,\alpha)$  knockout process.

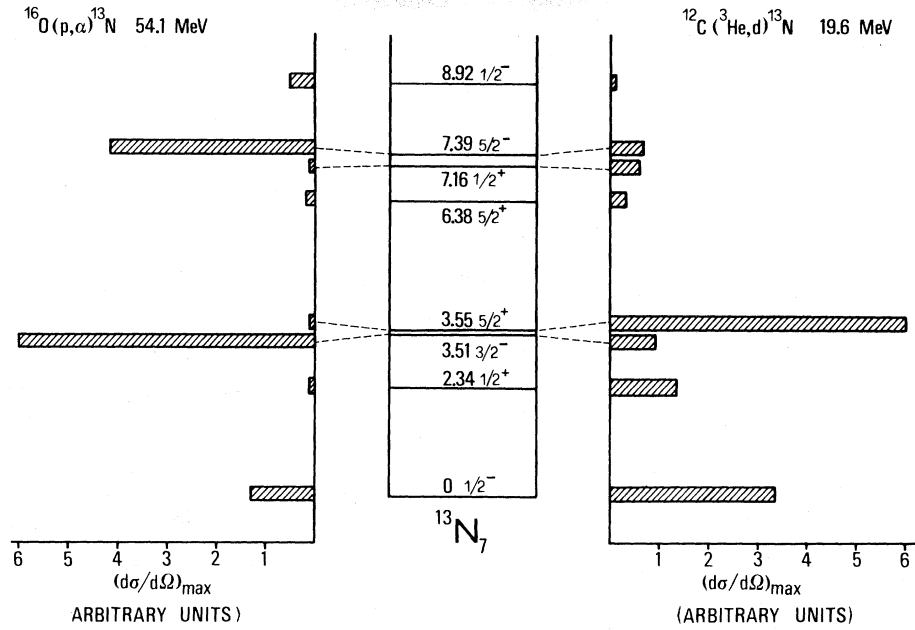


FIG. 10. Comparison of levels and differential cross sections observed in  $^{16}\text{O}(p,\alpha)^{13}\text{N}$  and  $^{12}\text{C}(^3\text{He},d)^{13}\text{N}$  reactions.

pens, as we can see from Fig. 13, for the  $J^\pi = \frac{3}{2}^+$  1.27 MeV,  $J^\pi = \frac{5}{2}^+$  2.23 MeV,  $J^\pi = \frac{1}{2}^+$  3.13 MeV,  $J^\pi = \frac{5}{2}^+$  3.26 MeV,  $J^\pi = \frac{7}{2}^-$  4.43 MeV,  $J^\pi = \frac{5}{2}^+$  4.73 MeV,  $J^\pi = \frac{3}{2}^+$  6.38 MeV, and  $J^\pi = \frac{3}{2}^-$  6.52 MeV states.

#### IV. SUMMARY

The present experiment has shown the importance of the pickup process in the dynamics of the (p, $\alpha$ ) reaction

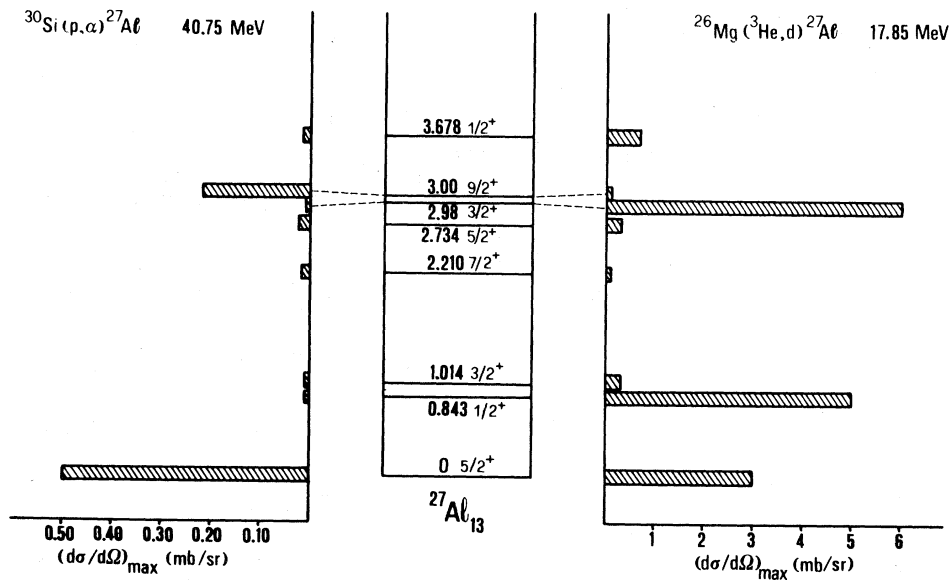


FIG. 11. Comparison of levels and differential cross sections observed in  $^{30}\text{Si}(p,\alpha)^{27}\text{Al}$  and  $^{26}\text{Mg}(^3\text{He},d)^{27}\text{Al}$  reactions.

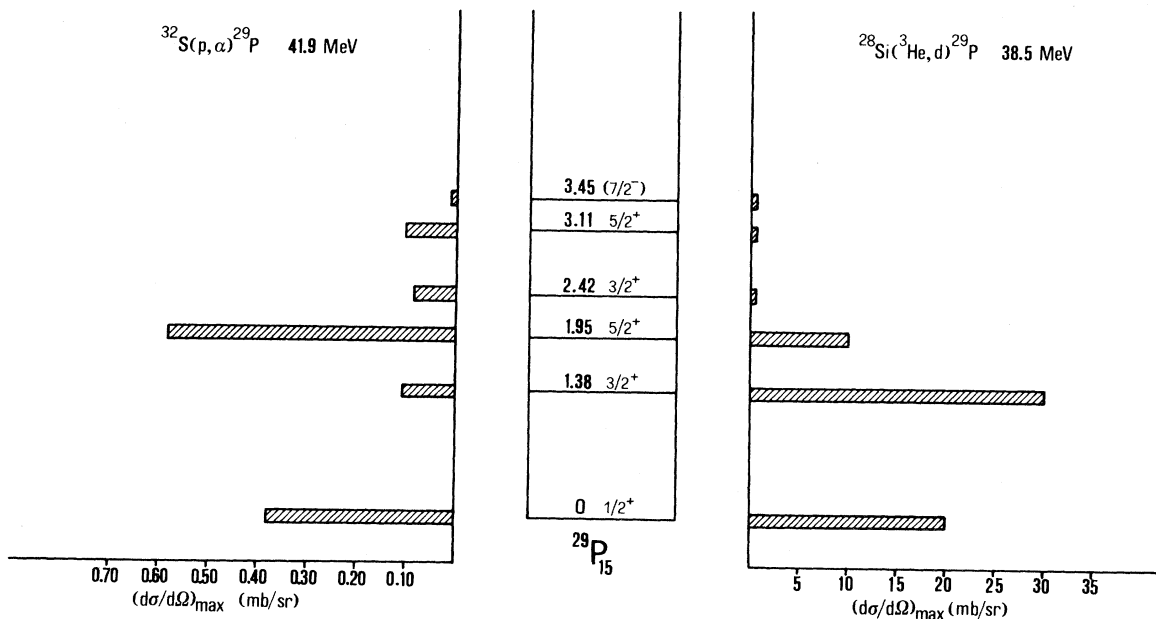


FIG. 12. Comparison of levels and differential cross sections observed in  $^{32}\text{S}(p, \alpha)^{29}\text{P}$  and  $^{28}\text{Si}(^3\text{He}, d)^{29}\text{P}$  reactions.

mechanism. A simplified analysis based on a semimicroscopic form factor with distorted wave direct pickup calculations, and using current shell model wave functions, reproduces fairly well the experimental results obtained in  $^{12}\text{C}(p, \alpha)^9\text{B}$  and  $^{32}\text{S}(p, \alpha)^{29}\text{P}$  reactions. A direct comparison

between  $(p, \alpha)$  and  $(^3\text{He}, d)$  spectra leading to the same final nucleus in the  $1p, 2s-1d$  nuclear region has shown peculiar differences. Of particular importance is the difference in the excitation of the same state in the  $(p, \alpha)$  and  $(^3\text{He}, d)$  spectra; that is, if a state is strongly excited in one reac-

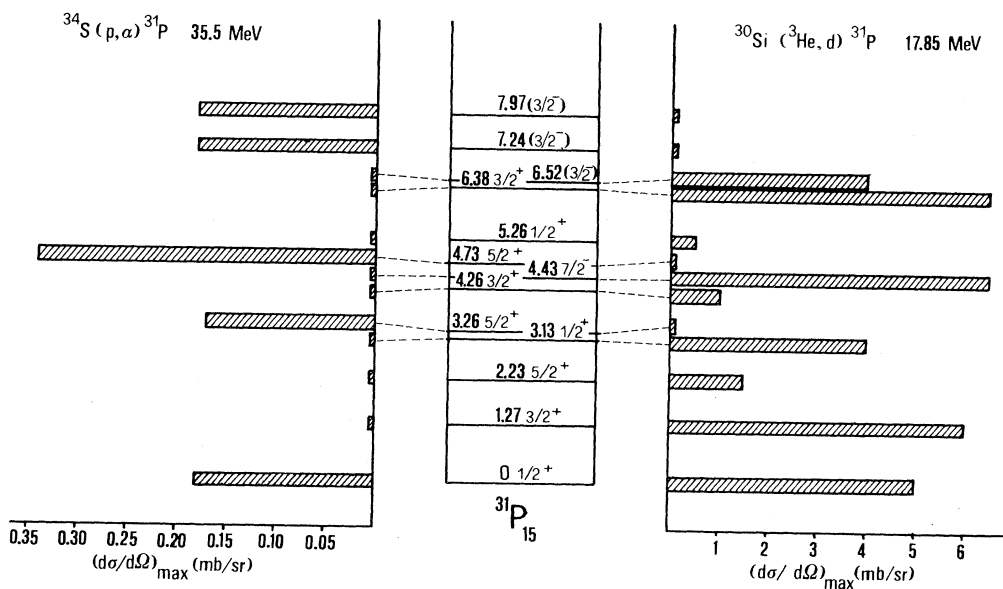


FIG. 13. Comparison of levels and differential cross sections observed in  $^{34}\text{S}(p, \alpha)^{31}\text{P}$  and  $^{30}\text{Si}(^3\text{He}, d)^{31}\text{P}$  reactions.

TABLE VII. Summary of results from the  $^{32}\text{S}(p,\alpha)^{29}\text{P}$  reaction.

| $E_x$ (MeV) | $J^\pi$         | $L$ | Integrated cross section   |   | Angular interval<br>of integration<br>(lab) |
|-------------|-----------------|-----|----------------------------|---|---|
|             |                 |     | Expt.<br>( $\mu\text{b}$ ) | Calc. <sup>a</sup><br>( $\mu\text{b}$ ) |   |
| 0           | $\frac{1}{2}^+$ | 0   | 156 $\pm$ 24               | 142                                     | 10–68                                       |
| 1.38        | $\frac{3}{2}^+$ | (2) | 44 $\pm$ 22                | 6.3                                     | 10–60                                       |
| 1.95        | $\frac{5}{2}^+$ | 2   | 448 $\pm$ 68               | 472                                     | 10–68                                       |
| 2.42        | $\frac{3}{2}^+$ | (2) | 34 $\pm$ 17                | 49                                      | 10–60                                       |
| 3.11        | $\frac{5}{2}^+$ | (2) | 42 $\pm$ 21                | 34                                      | 10–60                                       |

<sup>a</sup>The calculated cross section has been integrated in the same angular interval as the experimental one using a normalization factor  $D=480$ . For the transitions with  $L$  in parentheses, the experimental integrated cross sections have to be interpreted as upper limits, because of low statistics.

tion, it is weakly excited in the other and vice versa. This peculiar aspect confirms the dominance of the pickup process in the dynamics of the (p, $\alpha$ ) reaction as compared to the stripping process which dominates the ( $^3\text{He},d$ ) reactions. The knockout process with the approximation of the “ $\alpha$  spectator model” should have shared with the ( $^3\text{He},d$ ) reaction the same single proton transfer feature.

#### ACKNOWLEDGMENTS

The authors wish to thank Dr. S. S. Ahmad for his interest and suggestions throughout the progress of this work. They also wish to acknowledge Mr. A. Dal Bello for his assiduous assistance during the experiment.

<sup>1</sup>F. Pellegrini, G. Calvelli, P. Guazzoni, and S. Micheletti, Phys. Rev. C **15**, 573 (1977).

<sup>2</sup>F. Pellegrini, G. Calvelli, P. Guazzoni, and S. Micheletti, Phys. Rev. C **18**, 613 (1978).

<sup>3</sup>F. Pellegrini, G. Calvelli, D. Trivisonno, and P. Guazzoni, Phys. Rev. C **26**, 441 (1982).

<sup>4</sup>C. Maples and J. Cerny, Phys. Lett. **38B**, 504 (1972).

<sup>5</sup>T. Y. Li and B. Hird, Phys. Rev. **174**, 1130 (1968).

<sup>6</sup>S. Cohen and D. Kurath, Nucl. Phys. **73**, 1 (1975).

<sup>7</sup>D. Amit and A. Katz, Nucl. Phys. **58**, 388 (1964).

<sup>8</sup>B. H. Wildenthal, J. B. McGrory, E. C. Halbert, and H. D. Graber, Phys. Rev. C **4**, 1708 (1971).

<sup>9</sup>B. H. Wildenthal and J. B. McGrory, Phys. Rev. C **7**, 714 (1973).

<sup>10</sup>H. T. Fortune, T. J. Gray, W. Trost, and N. R. Fletcher, Phys. Rev. **179**, 1033 (1969).

<sup>11</sup>H. F. Lutz, D. W. Heikkinen, W. Bartolini, and T. H. Curtis, Phys. Rev. C **2**, 981 (1970).

<sup>12</sup>R. J. Peterson and R. A. Ristinen, Nucl. Phys. **A246**, 402 (1975).